Valence band structure and effective masses of GaN(10$\bar{1}$0)

Martin Franz,[1,*] Stephan Appelfeller,[1] Holger Eisele,[1] Philipp Ebert,[2] and Mario Dähne[1]
[1]*Institut für Festkörperphysik, Technische Universität Berlin, 10623 Berlin, Germany*
[2]*Peter Grünberg Institut, Forschungszentrum Jülich GmbH, 52425 Jülich, Germany*

(Received 10 August 2017; revised manuscript received 22 March 2019; published 17 May 2019)

The electronic structure of the clean and stoichiometric GaN(10$\bar{1}$0) cleavage surface is investigated in a comprehensive angle-resolved photoelectron spectroscopy study. A clear distinction between surface and bulk related features allows us to measure the dispersions of the occupied surface state band from the N dangling bonds as well as of the uppermost bulk valence bands and to extract the effective hole masses directly with high precision. This is performed along various directions in $k_{\parallel}$ space providing a detailed picture of the electronic band dispersion. The obtained results show three separated bulk bands without indications of a crossing of these bands as commonly predicted in theoretical works. Moreover, from the observed Fermi-level pinning we determine the position of the minimum of the empty Ga-derived surface state band, which is found deep within the fundamental band gap at ∼2.3 eV above the valence band maximum.

DOI: 10.1103/PhysRevB.99.195306

I. INTRODUCTION

GaN and related group III-nitride semiconductors became the material system of choice for optoelectronics, lighting, and high power electronics. Despite the extraordinary importance of GaN, its fundamental properties are still poorly known. For example, the effective hole masses and the shape of the valence band states is still highly debated. Most values originate from calculations of the electronic band structure [1–11], while only limited experimental data are available [12–21]. In addition, the situation is aggravated by the rapid improvement of the quality of GaN epitaxial layers and pseudosubstrates since the first demonstration of a blue LED, which led to experiments on widely differing material qualities. Moreover, the experimental values are based on optical methods (almost exclusively photoluminescence spectroscopy), which, as indirect methods, require assumptions for extracting effective masses. Although the most direct experimental method would be a band dispersion measurement by angle resolved photoelectron spectroscopy (ARPES), such experiments were not used to extract effective masses [22–32]. As a consequence, this situation led to widely varying experimental values for the effective masses, e.g., ranging from 0.54 m_0 to 2.2 m_0 for the heavy hole mass in the Γ-A direction ($m_{\mathrm{A}}^{\Gamma-\mathrm{A}}$) [15,17]. Also the corresponding theoretical values exhibit a significant spread, i.e., 1.1 m_0 to 2.09 m_0 [1,2,4]. Hence, the effective hole masses need to be revisited. Therefore, we conducted a comprehensive ARPES study of the GaN(10$\bar{1}$0) surface in order to map the dispersions of the uppermost bulk valence bands and the filled N-derived surface state S_{N} and to extract the effective hole masses directly with high precision.

II. EXPERIMENTAL

The angle-resolved photoelectron spectroscopy measurements were carried out at the UE56/2 PGM-1 beamline at BESSY II using a SPECS PHOIBOS 100 electron analyzer equipped with a two-dimensional CCD detector. The position of the Fermi energy (E_{F}) was calibrated using a clean Au foil in direct electrical contact with the GaN sample.

In order to probe the bulk valence band dispersion without adverse effects from surface reconstructions and contaminations, such as Ga adlayers on polar GaN surfaces [33], we investigated freshly cleaved, clean, and stoichiometric nonpolar GaN(10$\bar{1}$0) *m*-plane surfaces. For the experiments, samples cut from GaN(0001) pseudosubstrates [*n*-type, (1–3) × 10^{18} cm^{-3}] were electrically contacted by a sputtered Au film. A notch initiated the *in situ* cleavage in ultrahigh vacuum ($p < 10^{-8}$ Pa). A representative scanning tunneling microscopy (STM) image of such a surface is shown in Fig. 1(a) illustrating that the cleavage results in GaN(10$\bar{1}$0) surfaces with large, atomically flat terraces [34–36]. Furthermore, the overview photoelectron spectrum in Fig. 1(b) demonstrates that the cleaved GaN surface is clean and stoichiometric. No C is detected, while the minute O signal is attributed to the oxidized GaN regions surrounding the cleavage surface, since the beam diameter of ∼90 μm slightly exceeds the width of the cleavage surface of ∼80 μm.

III. RESULTS AND DISCUSSION

A. Distinction of bulk and surface bands

Figures 2(a) and 2(b) show the dispersion along the $\overline{\Gamma}$-$\overline{\mathrm{X}}'$ direction of the surface Brillouin zone (SBZ) [see Fig. 2(g)] measured by ARPES with a photon energy of 62 eV. The most dominant ARPES intensity, indicated by a red dotted line in (b), is assigned to a bulk band since it is not affected by surface degradation. Besides this band, additional bulk bands are found (marked by red dash-dotted lines).

In contrast, a weakly dispersing state appears as a distinct shoulder (indicated by blue dashed lines). This electron state is visible in particular at the boundary of the SBZ around the $\overline{\mathrm{X}}'$ point, while it is superposed by the strong emission from

*martin.franz@physik.tu-berlin.de

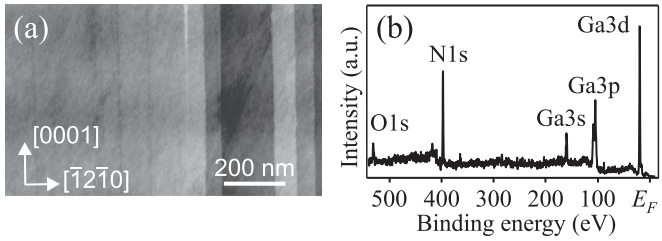

FIG. 1. (a) Overview STM image of the GaN(10$\bar{1}$0) cleavage surface, taken at a sample voltage of +5.9 V and a tunneling current of 80 pA. (b) Overview photoelectron spectrum ($h\nu = 800$ eV).

the aforementioned bulk band around the $\overline{\Gamma}$ point. Its intensity gradually disappears due to surface degradation, clearly identifying it as a surface state. Moreover, the dispersion of only ∼0.2 eV fits well to the almost vanishing dispersion of the N-derived dangling bond surface state S_N found in theoretical calculations [26,37–40]. Thus, this electronic state in the ARPES spectra is assigned to the filled N-related surface state band.

Since the surface sensitivity of ARPES depends on the used photon energy and the photoelectron emission process is always affected by matrix element effects, the photon energy was systematically varied between 62 eV and 100 eV. In this way, the optimum experimental conditions regarding the visibility of the S_N surface state band were found for $h\nu = 80$ eV, as shown in Figs. 2(c)–2(f). In comparison with the situation at $h\nu = 62$ eV, the dominant bulk signal that masked the surface state around the $\overline{\Gamma}$ point is now shifted to higher binding energies [Figs. 2(c) and 2(d)]. Hence, the dispersion of S_N in the central region of the SBZ becomes visible. In addition, due to the higher photon energy a larger section of the SBZ can be measured with the CCD detector, almost up to the $\overline{X}$ point [Figs. 2(e) and 2(f)]. However, along this direction the dispersion of S_N is again superimposed around the $\overline{\Gamma}$ point by intense and energetically close bulk bands. In all cases we observe only one surface state band with maximum at the $\overline{\Gamma}$ point. This is in contrast to a previous ARPES measurement, which, however, did not provide any experimental distinction of surface and bulk states [26].

The deviation in the appearance of the bulk valence band structure between $h\nu = 62$ eV and $h\nu = 80$ eV is related to different $k_\perp$ values for the different photon energies as well as to matrix element effects. At $h\nu = 62$ eV, we probe the bulk Γ point in normal emission geometry, taking into account an inner potential of 15 eV relative to the valence band maximum (VBM) [32]. In contrast, the measurement at $h\nu = 80$ eV probes a k point roughly at 40% along the Γ-M line.

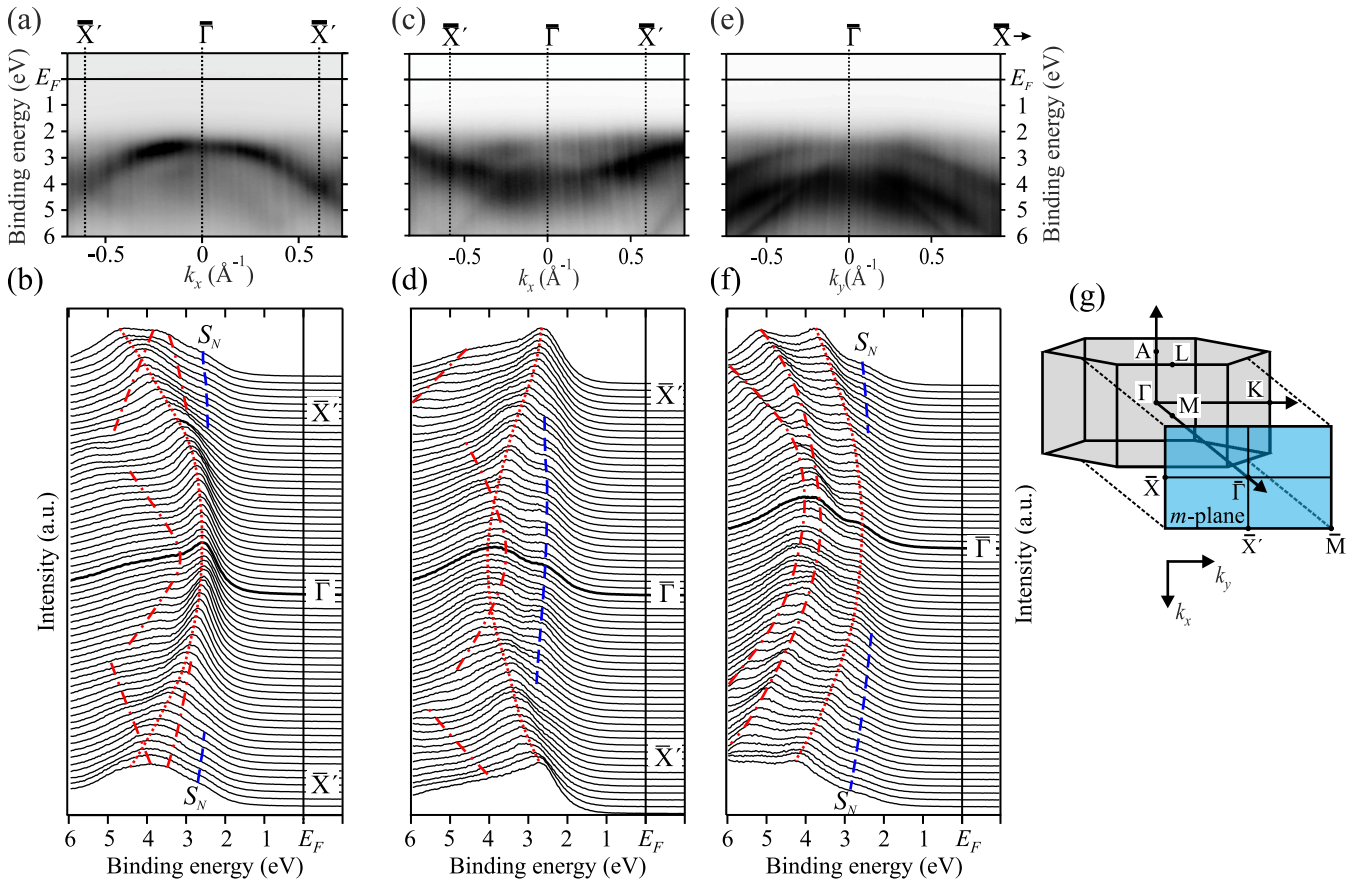

FIG. 2. ARPES results for (a),(b) $h\nu = 62$ eV and (c)–(f) $h\nu = 80$ eV measured along (a)–(d) the $\overline{\Gamma}$-$\overline{X}'$ and (e),(f) the $\overline{\Gamma}$-$\overline{X}$ directions. The blue lines indicate the dispersion of the surface state band S_N, while the red lines indicate bulk bands. (g) Relation between the wurtzite bulk Brillouin zone (gray) and the SBZ of the (10$\bar{1}$0) surface (m-plane, blue).

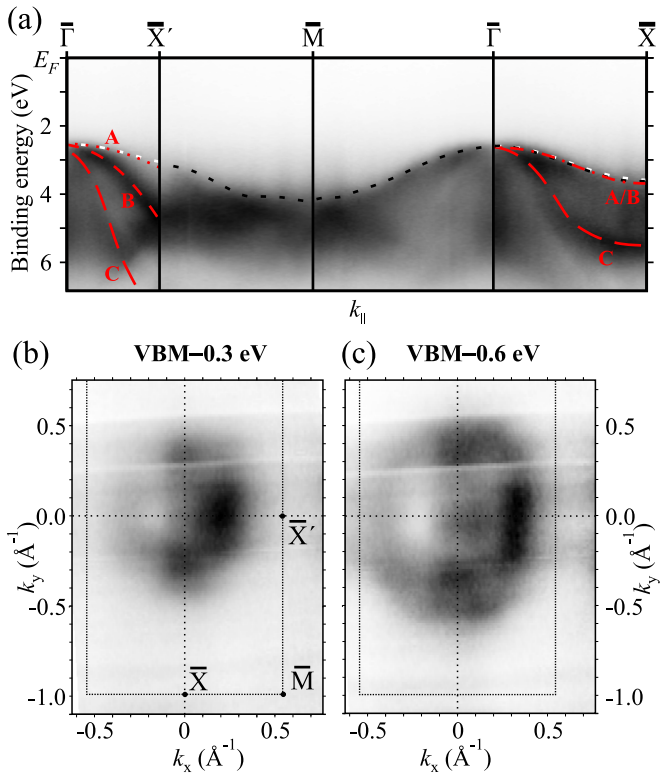

FIG. 3. (a) Bulk dispersion along the $\overline{\Gamma}$-$\overline{X}'$-$\overline{M}$-$\overline{\Gamma}$-$\overline{X}$ path ($h\nu$ = 62 eV). The red dashed and dotted lines indicate the bulk bands analyzed in this work. The black and white dashed lines show the calculated projection of the upper valence band edge taken from Refs. [39] and [40], respectively. (b),(c) Energy surfaces at (b) 0.3 eV and (c) 0.6 eV below the VBM. The asymmetry of the intensity distribution is related to matrix element effects.

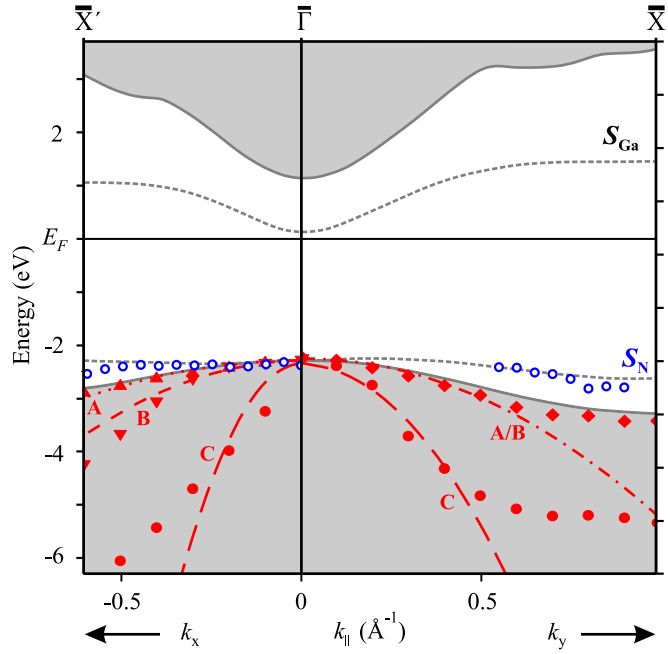

FIG. 4. Comparison of the experimentally determined band structure (symbols) with the calculated band structure taken from Ref. [40]. The calculated projected bulk band structures are shown as gray areas, whereas the surface state bands are indicated as dashed gray lines. The blue open circles show the experimental dispersion of S_N taken at $h\nu = 62$ eV and $h\nu = 80$ eV. The bulk valence bands taken at $h\nu = 62$ eV are indicated by red solid symbols, and the red dashed and dotted lines are parabolic fits to the measured bulk bands around the $\overline{\Gamma}$ point.

B. Valence band structure

A further ARPES measurement on a different GaN($10\bar{1}0$) cleavage surface is shown in Fig. 3. In contrast to the previously discussed cases, a scan of the complete two-dimensional $k_\parallel$ space was performed here, resulting in a three-dimensional data set, providing the dispersion along any direction, as shown exemplarily in Fig. 3(a) for the directions between the high-symmetry points. Additionally, also energy surfaces can be extracted, as shown in Figs. 3(b) and 3(c) for binding energies of 0.3 eV and 0.6 eV below the VBM, respectively. Due to the already mentioned degradation of the sample caused by the considerably longer acquisition time for this measurement, the S_N surface state band has already disappeared and is no longer visible in Fig. 3. This enables a detailed analysis of the dispersion of the uppermost bulk valence bands.

Three bulk bands are identified in the ARPES data along the $\overline{\Gamma}$-$\overline{X}'$ direction, as indicated by red lines in Fig. 3(a). At this point, a reliable assignment to the heavy hole, light hole, and the crystal-field split-off bands is difficult. Thus, the band with the weakest dispersion and thus the largest effective mass is named band A, the one with an intermediate effective mass band B, and the most strongly dispersing one band C. In contrast, only two bulk bands are identified along the $\overline{\Gamma}$-$\overline{X}$ direction. The observation of two bulk valence bands instead of three is assigned to rather similar effective masses for bands A and B along the Γ-K direction.

Moreover, the calculated projection of the upper valence band edge [39,40] is shown as black and white dashed lines in Fig. 3(a). It agrees very well with the intensity cutoff of the experimental band structure.

As the measurement shown in Fig. 3 provides the pure bulk dispersion around the Γ point, it is used for a detailed analysis of the bulk band structure and in particular of the effective hole masses. For this purpose, intensity profiles like those shown in Figs. 2(b), 2(d), and 2(f) are analyzed in detail to extract the dispersion curves. A summary of the dispersions of bulk and surface states derived from ARPES and a comparison with band structure calculations from Ref. [40] are shown in Fig. 4.

Now, we turn to the dispersion of the filled surface state S_N, which is derived from the measurements at $h\nu = 62$ eV and $h\nu = 80$ eV shown in Figs. 2(a)–2(f). As shown in Fig. 4, the surface state band S_N is located around the $\overline{\Gamma}$ point at or slightly below the VBM. Along the $\overline{\Gamma}$-$\overline{X}'$ direction, it first shows an almost vanishing dispersion around the $\overline{\Gamma}$ point, before it disperses downwards by ∼0.2 eV towards the $\overline{X}'$ point. In the $\overline{\Gamma}$-$\overline{X}$ direction, a larger downwards dispersion of ∼0.5 eV is observed. The observed dispersion of the S_N surface state agrees very well with band structure calculations from Ref. [40], shown as a dashed gray line in Fig. 4. The calculated surface state also exhibits a very weak dispersion

TABLE I. The effective hole masses of the bands around the Γ point, as derived from the parabolic fits to the observed bulk bands shown in Fig. 4, in comparison with experimental and theoretical literature data. The nomenclature of the bands is chosen in decreasing order of their effective masses. Literature values with a deviating assignment are marked with asterisks. All values are given in units of the free-electron mass m_0.

	$m_A^{\Gamma\text{-A}}$	$m_B^{\Gamma\text{-A}}$	$m_C^{\Gamma\text{-A}}$	$m_{A/B}^{\Gamma\text{-K}}$	$m_C^{\Gamma\text{-K}}$
This work	1.94 ± 0.25	0.97 ± 0.30	0.10 ± 0.08	1.27 ± 0.30	0.31 ± 0.20
Experiment					
Merz *et al.*[a]	0.54				
Im *et al.*[b]	2.2 ± 0.2				
Steube *et al.*[c]	$1.6 \pm 0.5^*$	1.1 ± 0.2	$1.0 \pm 0.1^*$		
Rodina *et al.*[d]	1.76 ± 0.30	0.42	0.30	$0.68^*/0.51$	0.35^*
Shields *et al.*[e]				1.8	
Feneberg *et al.*[f]	1.95			1.82/1.64	
Theory					
Suzuki *et al.*[g]	1.10	1.10	0.15	$1.65^*/1.10^*$	0.15^*
Chuang and Chang[h]	1.10	0.60	0.17	$0.77^*/0.30$	0.27^*
Chen *et al.*[i]	2.03	1.25	0.15	$1.22^*/0.34$	0.33^*
Majewski *et al.*[j]	2.09	0.74	0.18	$0.94^*/0.39$	0.37^*
Kim *et al.*[k]	2.00	1.17	0.15	$1.53^*/0.35$	0.33^*
Yeo *et al.*[l]	1.96	1.96	0.14	$1.96^*/1.87$	0.14^*
Persson *et al.*[m]	2.07	1.26	0.15	$1.14^*/0.33$	0.32^*
Carrier and Wei[n]	2.04	0.85	0.19	$1.05^*/0.43$	0.39^*
Rinke *et al.*[o]	1.88	0.92	0.19	$1.27^*/0.36$	0.33^*
Carvalho *et al.*[p]	2.00	1.22	0.20	$0.92^*/0.57$	0.31^*
Punya and Lambrecht[q]	1.85	0.55	0.20	$0.80^*/0.69$	0.50^*

[a]Reference [15]; [b]Ref. [17]; [c]Ref. [18]; [d]Ref. [19]; [e]Ref. [20]; [f]Ref. [21]; [g]Ref. [1]; [h]Ref. [2]; [i]Ref. [3]; [j]Ref. [4]; [k]Ref. [5]; [l]Ref. [6]; [m]Ref. [7]; [n]Ref. [8]; [o]Ref. [9]; [p]Ref. [10]; [q]Ref. [11].

around the $\overline{\Gamma}$ point for both directions in k space. However, in previous ARPES experiments [26], where only the dispersion along the $\overline{\Gamma}$-$\overline{X}'$ direction was studied, an energy minimum around $\overline{\Gamma}$ was found, indicating a holelike behavior [26]. As pointed out earlier, these ARPES results suffer from the lack of an experimental distinction between surface and bulk states, so that the reported apparent minimum at $\overline{\Gamma}$ could be due to an overlap of surface and more intense bulk bands.

C. Effective masses

From the dispersion of the observed bulk bands, the effective hole masses are determined by parabolic fits close to the $\overline{\Gamma}$ point, which are indicated by the dashed and dotted lines in Fig. 4. As shown in Fig. 2(g), the $\overline{\Gamma}$-$\overline{X}'$ direction corresponds to the bulk Γ-A direction and the $\overline{\Gamma}$-$\overline{X}$ direction to the bulk Γ-K direction. The obtained values are summarized in Table I. The nomenclature of the bands is thereby chosen in decreasing order of their effective masses, since a reliable assignment of the bands for the different directions is difficult at this stage, as pointed out earlier. In some cases, this differs from the assignments used in literature, where strong anisotropies of the effective masses are observed, e.g., with band C showing the smallest effective mass in the Γ-A direction but the largest in the Γ-K direction [1–11]. A more detailed discussion of the band assignment is presented below. The agreement of the obtained values with recent theoretical works is much better than for previous experimental data. This is attributed to the direct band structure measurement using ARPES, allowing a more precise extraction of the effective hole masses as compared to an indirect determination, e.g., using photoluminescence spectroscopy, which relies on additional information on the electron effective masses [17–19].

From the complete $k_\parallel$ space measurement, also effective masses along other directions are determined, allowing a better understanding of the dispersion and the properties of the bulk valence band structure. The results for the observed bulk bands measured along several polar angles are shown in Fig. 5(a). From the observed grouping of the data points, they can now be assigned to different bands as shown by the red lines. As can be already seen in Table I, band A shows a strong anisotropy with a larger effective mass along the Γ-A direction, while band B has rather similar effective masses around 1 m_0 for all polar angles. Regarding band C, our assignment suggests the smallest effective mass values for both the Γ-A and the Γ-K directions. However, this behavior is in contrast to the typical assignment reported in theoretical works [1–11], where band C has the smallest effective mass along the Γ-A direction but the largest along the Γ-K direction. For comparison, an alternative assignment taking the theoretical results into account is schematically drawn in Fig. 5(a) as gray lines. Such an assignment is only possible when band C crosses bands A and B. The effective mass plot determined here does not indicate such a crossing. However, a reliable statement on this issue is difficult on the basis of the effective mass plot alone.

Thus, we calculated the energy surfaces on the basis of the derived effective masses assuming a parabolic dispersion. The results are shown together with the experimental energy surfaces in Figs. 5(b) and 5(c) for 0.3 eV and 0.6 eV below the

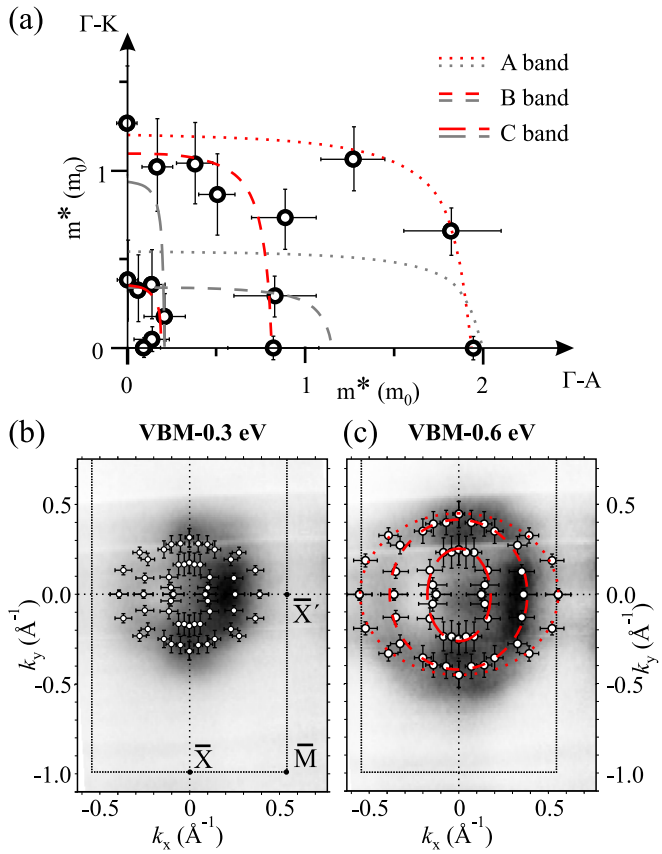

FIG. 5. (a) Polar plot of the effective masses for the bulk valence bands along different directions in $k_{\|}$ space obtained from a fit to the experimentally observed bands. The red lines show our assignment to the different bands, while the gray lines correspond better to an assignment in agreement with theory. (b),(c) Comparison between the measured energy surfaces at (b) 0.3 eV and (c) 0.6 eV below VBM, as already shown in Figs. 3(b) and 3(c), and those calculated from the effective masses. The red curves show the suggested shapes of the energy surfaces for the three bands.

VBM, respectively. For both energies, the data points show a good agreement with the observed photoelectron intensities. The distribution of the data points as well as the observed photoelectron intensities suggest a shape of the bands as indicated in (c) by the red ellipses. Thus, our data do not indicate any crossing of the bands, since band C in the Brillouin zone center is clearly separated by a region with lower photoelectron intensity from bands A and B.

Now the effective masses of the surface state S_N will be discussed. Its weak dispersion in both directions (see Fig. 4) results in rather large effective masses. For the $\overline{\Gamma}$-$\overline{X}'$ and $\overline{\Gamma}$-$\overline{X}$ directions, values of $9.4 \pm 2.0\ m_0$ and $5.6 \pm 2.0\ m_0$, are obtained, respectively. Thus far no other experimental or theoretical values of the effective mass of the surface state exist for comparison.

D. Fermi-level pinning and empty surface state

The sample degradation mentioned above does not only lead to the gradual disappearance of S_N but also to a variation in band bending, which needs to be considered to accurately determine the position of the VBM from the ARPES measurements and to accurately align the different measurements. This alignment was performed by an extrapolation of the Fermi-level position towards the situation of the freshly cleaved surface on the basis of the band bending determined from Ga3*d* core-level spectra. In this way, a binding energy of (2.3 ± 0.1) eV for the VBM with respect to E_F is obtained.

As the Ga-derived surface state S_{Ga} should primarily be responsible for the Fermi-level pinning in the present case of *n*-type GaN, the position of E_F found at 2.3 eV above the VBM (indicated in Fig. 4 by a black line) should correspond to the minimum of the S_{Ga} band at the $\overline{\Gamma}$ point. This clearly demonstrates that the empty Ga-derived surface state band reaches deep into the fundamental band gap.

Theoretical and experimental works disagree considerably regarding the energetic position of the S_{Ga} surface state band [39–45]. The position of the minimum of S_{Ga} at ∼2.4 eV above the VBM, as derived in Refs. [40,45], fits best to our data. Our ARPES data hence do not only provide information about the occupied band structure but also about the minimum of the S_{Ga} band.

IV. CONCLUSION

In conclusion, a comprehensive picture of the electronic properties of the GaN($10\overline{1}0$) surface was derived using ARPES. We mapped the dispersion of the bulk valence bands and of the occupied surface state band S_N and extracted the effective hole masses with high precision. The experimental energy surfaces do not indicate any crossing of the bulk bands, in contrast to suggestions by most theoretical works. Additionally, the position of the minimum of the empty surface state band S_{Ga} within the bulk band gap was deduced from the observed Fermi-level pinning. At the $\overline{\Gamma}$ point, the maximum of S_N is found close to the VBM and the minimum of S_{Ga} at ∼2.3 eV above the VBM.

ACKNOWLEDGMENTS

The authors thank V. Portz, M. Schnedler, A. Lenz, and C. Prohl for help with the sample preparation, L. Ivanova for performing the STM measurements, and J. Döhring for technical support during the beamtimes. K. Horn and Ch. Papp are acknowledged for providing the ARPES chamber and BESSY II (Helmholtz-Zentrum Berlin) for providing the beamtimes. This work was supported by the Deutsche Forschungsgemeinschaft, Sfb 787, TP A4.

[1] M. Suzuki, T. Uenoyama, and A. Yanase, Phys. Rev. B **52**, 8132 (1995).

[2] S. L. Chuang and C. S. Chang, Phys. Rev. B **54**, 2491 (1996).

[3] G. D. Chen, M. Smith, J. Y. Lin, H. X. Jiang, S.-H. Wei, M. A. Khan, and C. J. Sun, Appl. Phys. Lett. **68**, 2784 (1996).

[4] J. A. Majewski, M. Städele, and P. Vogl, MRS Proceedings **449**, 887 (1996).

[5] K. Kim, W. R. L. Lambrecht, B. Segall, and M. van Schilfgaarde, Phys. Rev. B **56**, 7363 (1997).

[6] Y. C. Yeo, T. C. Chong, and M. F. Li, J. Appl. Phys. **83**, 1429 (1998).

[7] C. Persson, A. F. da Silva, R. Ahuja, and B. Johansson, J. Cryst. Growth **231**, 397 (2001).

[8] P. Carrier and S.-H. Wei, J. Appl. Phys. **97**, 033707 (2005).

[9] P. Rinke, M. Winkelnkemper, A. Qteish, D. Bimberg, J. Neugebauer, and M. Scheffler, Phys. Rev. B **77**, 075202 (2008).

[10] L. C. de Carvalho, A. Schleife, and F. Bechstedt, Phys. Rev. B **84**, 195105 (2011).

[11] A. Punya and W. R. L. Lambrecht, Phys. Rev. B **85**, 195147 (2012).

[12] B. B. Kosicki, R. J. Powell, and J. C. Burgiel, Phys. Rev. Lett. **24**, 1421 (1970).

[13] R. Cunningham, R. Brander, N. Knee, and D. Wickenden, J. Lumin. **5**, 21 (1972).

[14] J. W. Orton, Semicond. Sci. Technol. **10**, 101 (1995).

[15] C. Merz, M. Kunzer, U. Kaufmann, I. Akasaki, and H. Amano, Semicond. Sci. Technol. **11**, 712 (1996).

[16] D. Volm, K. Oettinger, T. Streibl, D. Kovalev, M. Ben-Chorin, J. Diener, B. K. Meyer, J. Majewski, L. Eckey, A. Hoffmann, H. Amano, I. Akasaki, K. Hiramatsu, and T. Detchprohm, Phys. Rev. B **53**, 16543 (1996).

[17] J. S. Im, A. Moritz, F. Steuber, V. Härle, F. Scholz, and A. Hangleiter, Appl. Phys. Lett. **70**, 631 (1997).

[18] M. Steube, K. Reimann, D. Fröhlich, and S. J. Clarke, Appl. Phys. Lett. **71**, 948 (1997).

[19] A. V. Rodina, M. Dietrich, A. Göldner, L. Eckey, A. Hoffmann, A. L. Efros, M. Rosen, and B. K. Meyer, Phys. Rev. B **64**, 115204 (2001).

[20] P. A. Shields, R. J. Nicholas, F. M. Peeters, B. Beaumont, and P. Gibart, Phys. Rev. B **64**, 081203(R) (2001).

[21] M. Feneberg, M. Winkler, K. Lange, M. Wieneke, H. Witte, A. Dadgar, and R. Goldhahn, Appl. Phys. Express **11**, 101001 (2018).

[22] S. A. Ding, S. R. Barman, K. Horn, and V. L. Alperovich, *Proceedings of the 23rd Int'l Conference on the Physics of Semiconductors*, edited by M. Scheffler and R. Zimmermann (World Scientific, Singapore, 1996), p. 525.

[23] S. S. Dhesi, C. B. Stagarescu, K. E. Smith, D. Doppalapudi, R. Singh, and T. D. Moustakas, Phys. Rev. B **56**, 10271 (1997).

[24] T. Maruyama, Y. Miyajima, S. Cho, K. Akimoto, and H. Kato, Physica B **262**, 240 (1999).

[25] Y.-C. Chao, C. B. Stagarescu, J. E. Downes, P. Ryan, K. E. Smith, D. Hanser, M. D. Bremser, and R. F. Davis, Phys. Rev. B **59**, R15586 (1999).

[26] J. Wichert, R. Weber, L. Kipp, M. Skibowski, T. Strasser, F. Starrost, C. Solterbeck, W. Schattke, T. Suski, I. Grzegory, and S. Porowski, Phys. Status Solidi B **215**, 751 (1999).

[27] P. Ryan, Y.-C. Chao, J. Downes, C. McGuinness, K. E. Smith, A. V. Sampath, and T. D. Moustakas, Surf. Sci. **467**, L827 (2000).

[28] B. Kowalski, L. Pluciński, K. Kopalko, R. Iwanowski, B. Orowski, R. Johnson, I. Grzegory, and S. Porowski, Surf. Sci. **482-485**, 740 (2001).

[29] B. Kowalski, R. Iwanowski, J. Sadowski, J. Kanski, I. Grzegory, and S. Porowski, Surf. Sci. **507-510**, 186 (2002).

[30] L. Plucinski, T. Strasser, B. Kowalski, K. Rossnagel, T. Boetcher, S. Einfeldt, D. Hommel, I. Grzegory, S. Porowski, B. Orlowski, W. Schattke, and R. Johnson, Surf. Sci. **507-510**, 223 (2002).

[31] B. Kowalski, R. Iwanowski, J. Sadowski, I. Kowalik, J. Kanski, I. Grzegory, and S. Porowski, Surf. Sci. **548**, 220 (2004).

[32] S. M. Widstrand, K. O. Magnusson, L. S. O. Johansson, and M. Oshima, Surf. Sci. **584**, 169 (2005).

[33] J. E. Northrup, J. Neugebauer, R. M. Feenstra, and A. R. Smith, Phys. Rev. B **61**, 9932 (2000).

[34] H. Eisele, L. Ivanova, S. Borisova, M. Dähne, M. Winkelnkemper, and P. Ebert, Appl. Phys. Lett. **94**, 162110 (2009).

[35] P. H. Weidlich, M. Schnedler, H. Eisele, R. E. Dunin-Borkowski, and P. Ebert, Appl. Phys. Lett. **103**, 142105 (2013).

[36] M. Schnedler, V. Portz, H. Eisele, R. E. Dunin-Borkowski, and P. Ebert, Phys. Rev. B **91**, 205309 (2015).

[37] J. E. Northrup and J. Neugebauer, Phys. Rev. B **53**, R10477 (1996).

[38] C. G. Van de Walle and D. Segev, J. Appl. Phys. **101**, 081704 (2007).

[39] M. Landmann, E. Rauls, W. G. Schmidt, M. D. Neumann, E. Speiser, and N. Esser, Phys. Rev. B **91**, 035302 (2015).

[40] L. Lymperakis, P. H. Weidlich, H. Eisele, M. Schnedler, J.-P. Nys, B. Grandidier, D. Stiévenard, R. E. Dunin-Borkowski, J. Neugebauer, and P. Ebert, Appl. Phys. Lett. **103**, 152101 (2013).

[41] L. Ivanova, S. Borisova, H. Eisele, M. Dähne, A. Laubsch, and P. Ebert, Appl. Phys. Lett. **93**, 192110 (2008).

[42] M. Bertelli, P. Löptien, M. Wenderoth, A. Rizzi, R. G. Ulbrich, M. C. Righi, A. Ferretti, L. Martin-Samos, C. M. Bertoni, and A. Catellani, Phys. Rev. B **80**, 115324 (2009).

[43] M. Himmerlich, A. Eisenhardt, S. Shokhovets, S. Krischok, J. Räthel, E. Speiser, M. D. Neumann, A. Navarro-Quezada, and N. Esser, Appl. Phys. Lett. **104**, 171602 (2014).

[44] D. Segev and C. G. V. de Walle, Europhys. Lett. **76**, 305 (2006).

[45] V. Portz, M. Schnedler, H. Eisele, R. E. Dunin-Borkowski, and P. Ebert, Phys. Rev. B **97**, 115433 (2018).